Prilling of fatty acid-API suspensions: processability and characterization

E. De Coninck[a], V. Vanhoorne[a], A. Elmahdy[b], M. Boone[c], G. Van Assche[d], D. Markl[e,f], C. Vervaet[a]

[a] Laboratory of Pharmaceutical Technology, Ghent University, Ghent, Belgium

[b] Department of Materials Science and Engineering, Ghent University, Zwijnaarde, Belgium

[c] UGCT – Radiation Physics, Dept. Physics and Astronomy, Ghent University, Ghent, Belgium

[d] Physical Chemistry and Polymer Science, Vrije Universiteit Brussel ,Brussels, Belgium

[e] Strathclyde Institute of Pharmacy and Biomedical Sciences, University of Strathclyde, Glasgow, United Kingdom

[f] EPSRC Centre for Innovative Manufacturing in Continuous Manufacturing and Crystallisation, University of Strathclyde, Glasgow, UK

ABSTRACT

Current study evaluated the processability and characteristics of prills made of an active pharmaceutical ingredient/fatty acid (API/FA) suspension instead of previously studied API/FA solutions to enlarge the application field of prilling. Metformin hydrochloride (MET) and paracetamol (PAR) were used as model APIs while both the effect of drug load (10% to 40%) and FA chain length (C14 to C22) were evaluated. Prevention of nozzle obstruction due to large or agglomerated API particles in the molten FA was achieved via API sieving while sedimentation during processing was avoid via equipment modifications. Finally, the API/FA suspensions were processable on lab-scale prilling equipment without thermal degradation, nozzle obstruction or sedimentation in function of processing time. The processability of API/FA suspensions was only limited by the viscosity of the molten mixture which was mainly affected by the size and shape of the API particles but independent of the FA chain length. A lower API particle size and aspect ratio, resulted in a higher amount of particle-particle interactions and consequently a higher viscosity at equal drug load. Current study also gained more insight in the solidification behavior of API/FA based formulations in liquid nitrogen via high speed camera analysis and rapid heat calorimetry. The collected prills were spherical (AR ≥ 0.898) with a smooth surface (sphericity ≥ 0.914) and a stable particle size of ± 2.3mm and 2.4mm for MET and PAR prills respectively, independent of the drug load and/or FA chain length. In vitro drug release evaluation revealed a faster drug release at higher drug load, higher API water solubility and shorter FA chain length. Except for a 10% MET in behenic acid (C22) formulation since the low viscosity of the mixture resulted in an inhomogeneous API distribution in the prill, while stearic acid (C18) based formulations had an increased drug release due to their high porosity. Solid state characterization via XRD and Raman spectroscopy proved the preservation of API and FA crystallinity after thermal processing via prilling and during storage. Evaluation of the similarity factor proved a stable drug release (f_2 >50) of both MET and PAR prills after storage at 25°C or 40°C for 6 months.

KEYWORDS

Prilling

Controlled release

Multiparticulate dosage forms

Fatty acids

Metformin hydrochloride

Paracetamol

ABBREVIATIONS

API	active pharmaceutical ingredient
BA	behenic acid
FA	fatty acid
fps	frames per second
MA	myristic acid
MET	metformin hydrochloride
MPT	metoprolol tartrate
NA	not applicable
PA	palmitic acid
PAR	paracetamol
RH	relative humidity
RHC	rapid heat cool calorimeter
SA	stearic acid
SD	standard deviation
SEM	scanning electron microscopy
SLS	sodium lauryl sulfate
SNV	standard normal variate
TGA	thermogravimetric analysis
USP	United States Pharmacopeia
XRD	X-ray diffraction

TABLE OF CONTENTS

1. INTRODUCTION

Lipids (e.g. oils, waxes, triglycerides, partial glycerides, fatty alcohols and fatty acids (FAs)) gain interest in the pharmaceutical industry as excipients to mask taste, protect unstable active pharmaceutical ingredients (APIs), increase the bioavailability and sustain the dissolution rate, due to their biocompatibility, low toxicity, low cost and pharmaceutical approved status [1-6].

Solid lipid-based oral pharmaceutical drug formulations can be produced via different solvent-free melting techniques such as melt extrusion, melt coating and spray congealing. In comparison with the polymer industry, no solvents are used during these pharmaceutical production processes, resulting in relatively short, cost-effective and environmentally friendly production processes [3, 5-7]. Via spray congealing perfectly spherical microspheres consisting of a drug imbedded in a lipid matrix can be produced [8-9]. A specific type of spray congealing, called prilling, yields larger spherical particles (>500µm) resulting in a slower controlled release system and excellent flow properties for volumetric capsule filling [2, 5, 10-11].

Although prilling is widely applied in the agricultural industry for the production of urea beads, its applications in the pharmaceutical field are limited [12-15]. Pivette et al. examined the controlled-release mechanism of a highly water-soluble API from lipid microspheres composed of Compritol 888 and paraffin wax [1]. Vervaeck et al. demonstrated that long chain FAs, such as stearic acid (SA) and behenic acid (BA), are excellent matrix formers in a multiparticulate controlled release dosage form manufactured by prilling [11]. As the API can be dissolved or suspended in a (mixture of) molten FA during processing, the physical state of the drug during prilling could affect processing as well as the characteristics of the prills. As Vervaeck et al. focused on API/FA solutions (e.g. metoprolol tartrate (MPT) in BA), no information is available on the feasibility of prilling API/FA suspensions as indicated by Séquier et al. [7, 10]. Therefore the aim of current study was to evaluate the potential of prilling for APIs suspended in molten FA. Additionally, the MPT in BA formulations studied by Vervaeck et al, were further investigated in this study, to fully understand the effect of the presence of suspended versus dissolved API particles in the molten FA during processing [7, 11].

In the first part of this study, the processability of API/FA suspensions via prilling was evaluated. An API/FA suspension was defined as processable when prills could be generated without thermal degradation, nozzle obstruction or sedimentation during processing at a sufficiently high drug load. The second part of this study characterized the final prills in terms of size, shape, solid state and dissolution profile. Droplet formation at the nozzle and its solidification in liquid nitrogen was visualized via a high speed camera and quantified via rapid heat cool calorimetry (RHC). For the study two good water soluble APIs, metformin hydrochloride (MET) and paracetamol (PAR), which are insoluble in molten FA were selected to evaluate prilling with API/FA suspensions. Both the effect of drug load (10% to 40%) and FA chain length (C14 to C22) on the processability and prill characteristics were evaluated.

2. MATERIALS AND METHODS

2.1. MATERIALS

Four long chain saturated FAs with different carbon chain lengths (C14, C16, C18 and C22) were evaluated: myristic acid (MA) with a C14 purity of 99.2%, palmitic acid (PA) with a C16 purity of 99.3% and SA with a C18 purity of 98.3% (Mosselman, Ghlin, Belgium). BA was purchased from Oleon (Radiacid 0560, Ertvelde, Belgium) and had a C22 purity of 88.9%. The melting point of MA, PA, SA and BA is 53°C, 62°C, 68°C and 75°C, respectively. These FAs were combined with MET (Granules, Hyderabad, India), PAR (Mallinckrodt, Manchester, UK) or MPT (Esteve Quimica, Barcelona, Spain) as model drugs with a water solubility, of respectively 308 g/l (25°C), 17 g/l (30°C) and 682 g/l (20°C) [16-17]. Prills were dissolved in absolute (> 99.8%) ethanol (VWR, Leuven, Belgium). Dissolution media were made with sodium lauryl sulfate (SLS) (Fagron, Waregem, Belgium), potassium dihydrogen phosphate (VWR, Radnor, United States), sodium hydroxide (Sigma Aldrich, Saint Louis, United States) and hydrochloric acid (VWR, Radnor, United States).

2.2. METHODS

2.2.1. Prilling

Prills were manufactured using a modified Prilldrop® device (Peira, Turnhout, Belgium), depicted in Fig. 1. FAs were heated to 30°C above their melting temperature and subsequently the API was added to the molten FA under continuous stirring. After 15 min of intensive stirring at a constant temperature, the prilling process was started by applying an initial pressure (1 bar) on the reservoir to feed the viscous API/FA suspension to the thermostated nozzle (T_{nozzle} = $T_{melt\ FA}$ + 30°C; inner nozzle diameter: 0.445 mm). Subsequently the flow rate through this nozzle was controlled with a pneumatic valve system with a calibrated drop time for non-viscous pure water. Individual API/FA droplets were formed at the nozzle by lowering the pressure on the vessel (0.1 bar) and adjusting the valve opening (drop time: 0.03 s; interval: 0.10 s). Under these conditions, approximately 150 API/FA suspension droplets/min were formed at the nozzle. The individual droplets were quench cooled in liquid nitrogen whereby a solid matrix system (prill) was formed.

The effect of drug load (10% to 40%) and FA chain length (C14 to C22) on the processability of API/FA suspensions and the characteristics of prills was evaluated, manufacturing 12 different formulations (Table 1). All formulations were produced in duplicate to evaluate the drug content, solid state as well as size and shape of the prills for two independent batches while the dissolution profile after manufacturing and during storage was evaluated for one batch.

2.2.2. Thermogravimetric analysis (TGA)

Thermal stability of pure FAs and APIs under extreme processing conditions (i.e. 2 h at 105°C) was checked using TGA (Hi-res TGA 2950, TA instruments, Leatherhead, UK). The samples (± 15 mg) were heated to 110°C and kept isothermal for 2 h while recording the weight loss.

2.2.3. Hot stage microscopy

The solubility of MET and PAR in molten FAs was determined via hot stage microscopy (Leica, Wetzlar, Germany). Therefore, a physical mixture (≤ 180 µm) of 1% API in FA was filled in a quartz crucible (diameter: 15 mm) and heated to 30°C above the melting temperature of the FA. The API was defined as insoluble in the molten FA when API crystals were still visible (magnification: 100x) after maintaining the physical mixture at the maximum processing temperature ($T_{melt\ FA}$ + 30°C) for 1 h.

2.2.4. Rapid heat cool calorimetry (RHC)

To evaluate the crystallization kinetics of API/FA solutions and suspensions, a prototype RHC (TA Instruments, Leatherhead, UK) equipped with a liquid nitrogen cooling was used. A Tzero calibration was performed at 250°C/min with sapphire disks while an indium standard was

used for the temperature and enthalpy calibration. ±200 µg of pure FA or physical mixtures (particle size ≤125µm) were filled in a low mass (≤ 2.1mg) aluminum RHC crucible. As a pre-treatment in accordance with the prilling process, all samples were kept 30°C above the melting temperature of the used FA for 10 min to ensure complete melting of the FA and sufficient time for the MPT crystals to dissolve. Subsequently, the sample was rapidly cooled (250°C/min) to one of the crystallization temperatures (68.0°C, 69.0°C, 70.0°C, 70.5°C, 71.0°C, 71.5°C and 72.0°C) and kept isothermal for 2 min. Thereafter the sample was cooled down (500°C/min) to -50°C and a new pre-treatment was started. The time needed to reach the FA crystallization peak maximum when the crystallization temperature was reached, was used to compare the crystallization rate of the samples.

2.2.5. Size and shape of the suspended APIs

Since API particles and/or agglomerates can obstruct the nozzle, particle size and shape distribution of the suspended APIs was determined. The particle size and shape of the dry API powder was analysed via a dynamic image analyser (Camsizer XT, Retsch Technology, Haan, Germany) equipped with an air pressure dispersion unit set at 180 - 185 kPa (X-jet, Retsch Technology, Haan, Germany). Powders were analysed in triplicate to calculate the mean Feret diameter and weighted average aspect ratio (ratio of the minimal to the maximal Feret diameter) based on a volume distribution. Additionally, the shape of the dry API particles was visualized by scanning electron microscopy (SEM) (Quanta 200F, Thermo Fisher Scientific, Waltham, USA) after sputtering with a gold coating using the Emtech SC7620 sputter coater (Quorum Technologies, Laughton, United Kingdom) to improve the electron conductivity of the samples.

To evaluate API agglomeration in a hydrophobic environment such as molten FAs, laser diffraction (Malvern Mastersizer S long bench, Malvern Instruments, Malvern, UK) was applied on dispersions of the API in Miglyol 812® (IOI Oleo GmbH, Hamburg, Germany) which were vortexed and subsequently sonicated for 10 min. After transfer to the wet sample dispersion unit (1500 rpm) to obtain an obscuration of 10 - 30%, the samples were analysed using a 300RF lens (Malvern Instruments, Malvern, UK). d_{50} and d_{90} were determined on a volume based distribution after performing measurements in triplicate.

2.2.6. Drug content

Homogeneity of drug content in the prills as a function of processing time was assessed over a 1 h period at 6 min intervals. Drug content was spectrophotometrically determined using a double beam spectrophotometer (UV-1650PC, Shimadzu, Antwerp, Belgium) after dissolving ±35 mg prills (i.e. 5 prills) in absolute ethanol. MET concentrations were calculated based on a calibration curve ranging from 1.9 to 9.6 µg/ml at a wavelength of 239 nm. PAR concentrations were calculated based on a calibration curve ranging from 2.2 to 13.0 µg/ml at a wavelength of 250 nm. The deviation in drug content relative to the targeted drug content for each time interval and the weighted average drug content of the two independent batches of each formulation was calculated.

Via Raman microscopic mapping (Raman Rxn1 Microprobe, Kaiser Optical Systems, Ann Arbor, USA) the API distribution in the FA matrix was evaluated. Cross sections of prills were scanned in both the x and y directions with a 10x and 50x objective lens in area mapping mode using an exposure time of 5s with 3 accumulations and a step size of 50 µm and 10 µm, respectively. Data collection and data transfer were automated using HoloGRAMS™ data collection software (version 2.3.5, Kaiser Optical Systems, Ann Arbor, USA), the HoloMAP™ data analysis software (version 2.3.5, Kaiser Optical Systems, Ann Arbor, USA) and Matlab software (version 7.1, The MathWorks, Natick, MA, USA). Each mapping was evaluated via multivariate curve resolution (MCR) to evaluate the homogeneity of the API distribution in the FA matrix. Therefore, all spectra of each mapping were merged in a data matrix and baseline corrected via Pearson's method and subsequently normalized.

2.2.7. High speed camera

Droplet formation at the nozzle and their solidification in liquid nitrogen was visualized via a FASTCAM Mini AX200 high-speed camera (Photron, San Diego, USA) equipped with a 90 mm macro lens (Tamron, New York, USA). Resolution and frame rate (4000 – 6400 fps) were adjusted during the different experiments to obtain the best visualization of the event.

2.2.8. Size and shape of the prills

Surface and cross section of prills were examined by SEM (Quanta 200F, Thermo Fisher Scientific, Waltham, USA) after sputtering with a gold coating using the Emtech SC7620 sputter coater (Quorum Technologies, Laughton, United Kingdom) to improve the electron conductivity of the samples.

Size and shape (i.e. aspect ratio and sphericity) of the prills were evaluated via a dynamic imaging analysis technique (QICPIC, Sympatec, Clausthal-Zellerfeld, Germany). All batches (±2 g) were analysed in triplicate and Windox 5 software (Sympatec, Clausthal-Zellerfeld, Germany) was used to calculate the mean Feret diameter, weighted average aspect ratio (ratio of the minimal to the maximal Feret diameter) and sphericity (ratio of the perimeter of the equivalent circle, P_{EQPC}, to the real perimeter) based on a volume distribution. The average values of the two batches per formulation were reported.

2.2.9. Rheology of molten mixtures

The viscosity of pure FA and FA-API suspensions and solutions was measured using a controlled stress Haake™ Mars III rheometer (Thermo Fisher Scientific, Waltham, USA) with a 60 mm titanium parallel plate geometry. Depending on their viscosity, samples were analysed with flat, non-polished plates or serrated plates to obtain reliable rheological results that were not influenced by apparent wall slip or protrusion flow [18-19]. Via a Peltier temperature controller, the plate geometry was kept at the standard prilling processing temperature ($T_{melt,FA}$ + 30°C).

Pure FAs and molten FA-API suspensions and solutions were transferred to the plate geometry to obtain an appropriate gap of 2 ± 0.1 mm. In this way the gap was at least 10 times larger than the particle size of the suspended particles to ensure the presence of a continuous medium [20]. The shear rate was varied from 3000 s^{-1} to 0.1 s^{-1} or 500 s^{-1} to 0.01 s^{-1} in 15 steps (log scale) for measurements performed with flat or serrated plates, respectively. Each step was held for 30 s to give the sample enough time to stabilize and record an accurate torque value. Since sedimentation could occur during sample loading, the shear rate was varied from higher to lower values to obtain repeatable rheological results [19, 21]. All measurements were performed in triplicate and the average and standard deviation was calculated.

2.2.10. Solid state characterization

The solid state of pure components, physical mixtures (< 180 µm) and corresponding prills was analysed via XRD and Raman spectroscopy. X-ray diffraction patterns were recorded with a D5000 Cu Kα diffractor (ʎ = 0.154 nm) (Siemens, Karlsruhe, Germany) with a voltage of 40 mV in the angular range of 4° < 2θ < 60° using a step scan mode with step size of 0.02° and counting time of 1 s/step.
Raman spectra were recorded in triplicate with a Raman Rxn1 spectrometer (Kaiser Optical Systems, Ann Arbor, USA) equipped with an air-cooled CCD detector and a 785 nm Invictus NIR diode laser over the 0 – 1800 cm^{-1} range with a resolution of 4 cm^{-1}, an exposure time of 5 s and 3 accumulations. Data collection and data transfer were automated using HoloGRAMS™ data collection software (version 2.3.5, Kaiser Optical Systems, Ann Arbor, USA). Spectra were corrected by standard normal variate (SNV) pre-processing and centered prior to data analysis using Simca 14.1.0 (Umetrics, Umeå, Sweden).

2.2.11. In vitro drug release

In vitro dissolution tests were performed using USP dissolution apparatus 2 (paddle speed: 100 rpm) in combination with sinker baskets to prevent floating of the hydrophobic prills. The dissolution apparatus consisted of a VK 7010 dissolution system coupled to a VK 8000 automatic sampling station (Vankel, New Jersey, USA). Prills equivalent with 150 mg API (sink conditions) were added to 900 ml dissolution medium maintained at 37 ± 0.5°C. Four types of dissolution media were used to evaluate the influence of pH and/or surfactants on the drug release profile: demineralized water, phosphate buffer (pH 7.4), 0.1M HCl (pH 1) and 0.1% SLS aqueous solution. In case of dissolution tests on MET prills, 5 ml samples were withdrawn on 10 time points over a 5 h, 8 h or 12 h period, depending on the drug release rate. For dissolution tests on PAR prills, ten 5 ml samples were withdrawn during 24 h. Those samples were analyzed spectrophotometrically using a double beam spectrophotometer (UV-1650PC, Shimadzu, Antwerp, Belgium) to calculate the API concentration from a calibration curve ranging from 1.5 to 14.7 µg/ml at a wavelength of 234 nm for MET samples and from 1.7 to 16.9 µg/ml at 243 nm for PAR samples.

Similarity between dissolution profiles obtained in different media was evaluated by calculating the similarity factor f_2 as described by Shah et al. (Eq. 1) where R_t and S_t represent the cumulative drug release at sample point t of the sample in the reference medium and the sample in the alternative medium with n equal to the number of total sample points. As described by Shah et al. maximum one sample point with a cumulative drug release higher than 85% may be included to avoid bias in the similarity assessment. Therefore, depending on the drug release profile, 5 up to 10 sample time points were taken into account to calculate the similarity factor. Dissolution profiles are considered similar if f_2 is ≥ 50, based on average difference of 10% at all sampling time points [22].

$$f_2 = 50 \log_{10}\left\{\left[1 + \frac{1}{n}\sum_{t=1}^{n}(S_t - R_t)^2\right]^{-1/2} * 100\right\} \quad (1)$$

2.2.12. Storage

Since processing and storage of prills can change the crystalline state of formulation components and/or induce interactions at molecular level between the different components, a stability study was performed whereby the prills were packed immediately after production in hermetically sealed bags under controlled circumstances (< 35% RH) and stored at 25°C and 40°C for 1 week, 1 month, 3 months and 6 months [5, 23-25]. Beside evaluation of the solid state after storage, the drug release profile was re-evaluate throughout the stability study in demineralized water and 0.1% SLS solution for MET and PAR prills, respectively, by evaluation of the similarity factor.

2.2.13. X-ray tomography

Porosity and specific surface area of prills before and after dissolution was evaluated using high-resolution X-ray computed tomography (custom-designed mCT setup HECTOR of the Ghent University Centre for X-ray Tomography (UGCT)) for one batch per formulation [26]. An isotropic voxel size of 3.99 µm was used to analyse at least 15 prills per formulation.

The variation in the size of the cavity inside the prills was quantified by calculating the specific surface area of at least 10 prills of each formulation. The specific surface area was used to normalize for the small variation in particle size. Bespoke data processing was developed to determine the specific surface area of each prill from the 3D X-ray tomography data. Initially, the tomography images were denoised using an anistropic diffusion filter in order to improve the robustness of the subsequent steps. Thresholding was used to determine a binary volume from the denoised data. A marker-based Watershed algorithm was applied on the binary volume to separate the prills and facilitate the analysis of individual prills. The number of prills analysed is slightly smaller (i.e. up to 10 prills per formulation) than the total number of prills imaged as only prills visible in its entirety and clearly separated from each other were analysed.

3. RESULTS AND DISCUSSION

3.1. PROCESSABILITY

MET and PAR were selected as model APIs to evaluate the processability of API/FA suspensions since thermogravimetric analyses indicated no thermal degradation of these APIs or FAs under extreme processing conditions (i.e. 2h at 105°C), while hot stage microscopy demonstrated their insolubility in molten FA under the applied processing conditions (data not shown).

Prilling of API/FA suspensions initially resulted in obstruction of the 0.445 mm nozzle due to solidification of FA and/or (agglomeration of) the suspended particles. Solidification of molten FA in the nozzle was avoided by installing an extra heating pad around the nozzle of the prilling equipment (Fig. 1f). However, nozzle obstruction still occurred due to the presence of large MET crystals and agglomeration of the hydrophilic PAR in the molten hydrophobic FA, indicating that the mixing intensity during addition of the API to the molten carrier was insufficient to disperse PAR into its primary particles. This observation was confirmed by the larger API particle size (d_{50}) measured under wet conditions (i.e. dispersing PAR in a liquid phase with a hydrophobicity similar to FAs) in comparison to the d_{50} measured under dry conditions (Table 2). These PAR agglomerates were not even removed by the addition of a surfactant (0.2% polysorbate 80 or 0.2% sorbitan monolaurate in migylol® 812), ultrasonic vibration (4h – 40 kHz) or high shear mixing (10 min – 6000 rpm) in a Silverson L4R (East Longmeadow, United States). However, sieving of the API (using a 50 and 150 µm sieve for MET and PAR, respectively) prior to their addition to the molten FA was efficient to reduce the $d_{90\,wet}$ (≤ 60 µm) of the suspended particles and consequently preventing the blocking of the nozzle (445 µm) during processing (Table 2).

The design of the prilling device was also essential towards the quality of the prills. Whereas previous studies processed homogeneous API/FA solutions, this study focused on API/FA suspensions, which are intrinsically susceptible to sedimentation [11, 27]. Hence, it was essential to identify the critical parts of the equipment with a high probability of API sedimentation (e.g. due to inadequate flow or stirring) and to subsequently modify the process to ensure a constant drug content in the prills throughout the manufacturing process. While the flow inside the narrowed and shortened feed tubes towards the nozzle and inside the seamless nozzle (Fig. 2) was sufficient to avoid sedimentation of the suspended API, it was observed that the mixing intensity inside the reservoir remained the most critical parameter towards API sedimentation. Using sufficient mixing intensity in the reservoir yielded prills with a maximum relative drug content deviation below 15% for all time points per formulation, in accordance with the European Pharmacopoeia guidelines (Table 3) [28].

Initial screening experiments revealed that sieved (150 µm) PAR in BA suspensions were processable up to a drug load of 20%, while sieved (50 µm) MET in BA suspensions were processable up to a drug load of at least 40%. Since viscosity is a critical process parameter during droplet formation at the nozzle, this difference in maximum processable drug load could be attributed to the higher viscosity of PAR in BA suspensions in comparison with MET in BA suspensions at equal drug loads [10, 23]. Rheological experiments confirmed this hypothesis and revealed an almost Newtonian behaviour for MET suspensions while distinct shear thinning was observed for PAR suspensions (Fig. 3).

Since the measuring temperature was kept consistently 30°C above the melting temperature of the selected FA, varying the FA chain length of the formulations did not significantly change the viscosity (data not shown). Consequently, the observed differences in viscosity of MET and PAR formulations can be attributed to the varying size and shape of MET and PAR suspended particles. Sieved MET (50 µm) and PAR (150 µm) had a mean Feret diameter of 17 µm (span 1.84) and 13 µm (span 2.59), respectively (Table 2). Due to the lower particle size of PAR in comparison with MET, the number of particles and consequently the number of particle-particle interactions at equal drug load was higher in the PAR suspensions, resulting in a higher viscosity. Additionally, the degree of particle-particle interactions in PAR suspensions was favoured by the rod shape of PAR particles (AR: 0.765) in comparison with the more spherical MET particles (AR: 0.810) as demonstrated by SEM (Fig. 4). The elongated PAR particles had a higher barrier to start flow as a result of their larger specific surface area

and non-suitable particle orientation. As particle-particle interactions are weak forces, their effect was seen more at low shear rates what explained the shear thinning behaviour of the PAR formulations [21, 29-30].

Based on the initial screening experiments, formulations with a viscosity higher than that of the 20% PAR in BA suspension were defined as non-processable. These observations were in accordance with the measured viscosity of successfully processed MET (10 - 40%) in BA and 30% MPT in BA formulations. In conclusion, the processability of API/FA suspensions was dominated by the size and shape of the API powder and independent of the FA chain length. A lower API particle size and aspect ratio, resulted in a higher amount of particle-particle interactions and consequently a higher viscosity at equal drug load.

3.2. SIZE AND SHAPE OF THE PRILLS

SEM imaging revealed a characteristic structure of the MET and PAR prills, i.e. prills have an orifice at their surface which was connected to a cavity inside the prill (Fig. 5a,b). This phenomenon is independent of drug load, which is in contrast with MPT/FA solutions tested by Vervaeck et al [11]. MPT in BA prills with a low drug load (i.e. 10% and 20%) had an orifice and cavity such as all MET and PAR (API/FA suspensions) prills. When the drug load of this API/FA solution was increased up to 30% MPT in BA, the prills were completely solid and spherical despite an expulsion on their surface (Fig. 5c). To explain the observed differences in the final shape of suspension versus solution based prills, MPT in BA formulations as described by Vervaeck et al were further investigated in this study [7, 11, 31]. Visualization of the droplet formation at the nozzle of a 30% MPT in BA formulation and a 10% MET in BA formulation via a high speed camera revealed that the droplets became immediately (<11.6 ms and <22.8 ms) spherical when released from the nozzle (Fig. 6/7). This spherical shape was maintained during their falling motion before reaching the liquid nitrogen bath.

Consequently, the differences in prill shape originated from the droplet solidification in liquid nitrogen. The solidification of an opaque API/FA suspension droplet (Fig. 8) was initiated at a certain point (i.e. the point of origin) on the surface of the droplet and continued from here on in all directions eventually leaving a liquid area at the opposite site of the point of origin. The difference in cooling rate between the point of origin and the top of the sphere, led to an inhomogeneous shrinking process resulting in a stress field that created a cavity upon full solidification. These observations are in agreement with the characteristic shrinking properties of lipids during their crystallization [10, 32-33]. In contrast, the visualisation of droplet solidification of a transparent 30% MPT in BA solution revealed the creation of the expulsion at the surface of the final prills. The surface of the droplet solidified slowly from the point of origin while the unsolidified core of the droplet started to bulge as can be seen in Figure 9.

RHC experiments demonstrated that these observations were due to a different FA crystallization rate. Physical mixtures were pretreated 30°C above the melting temperature of the corresponding FA to simulate the first part of the prilling process before they were rapidly cooled down (250°C/min) and kept isothermal just below the melting point of the used FA. The time needed to reach the BA crystallization peak maximum during isothermal crystallization was comparable for all API/BA suspensions, independent of type of API or drug load (Fig. 10) in contrast to MPT in BA solutions. The higher the MPT drug load, the more time needed to reach the BA crystallization peak maximum. Since a 20% MPT in BA formulation still resulted in prills with a cavity, it was assumed that once a threshold crystallization rate was reached, between 20% and 30% MPT in BA, the droplet solidification was no longer dominated by the characteristic shrinking properties of FAs.

When analysing the final size and shape of API/FA suspension based prills (Table 4), no trends in function of drug load or FA chain length were detected. MET and PAR prills had a mean Feret diameter of 2.30 mm (span 0.10) and 2.42mm (span 0.08), an average aspect ratio of 0.905 ± 0.007 and 0.917 ± 0.012, and a sphericity of 0.937 ± 0.004 and 0.921 ± 0.007, respectively. Consequently, these spherical prills had good flow properties for easy filling into hard gelatin capsules for oral administration.

3.3. SOLID STATE CHARACTERIZATION

X-ray diffraction patterns demonstrated that the crystallinity of both MET, PAR and FAs did not change by thermal processing via prilling and during storage. Characteristic peaks of MET for 2θ (e.g. 12.2° and 17.7°) and PAR (e.g. 23.5° and 26.5°) showed up in the physical mixture and prills even after 6 months of storage, confirming that MET and PAR remained in their original crystalline form (data not shown). Stability of the FA crystallinity was in agreement with the observation of Kobayashi, who stated that molten FAs exclusively crystallized into the thermodynamically stable form C [34-35]. The absence of specific interactions between the components and the preservation of crystallinity during 6 months storage was confirmed via Raman spectroscopy since no changes in the characteristic Raman bands of MET, PAR and FAs were observed (data not shown).

3.4. IN VITRO DRUG RELEASE

A higher drug load of a hydrophilic API created an extensive channel network in a hydrophobic matrix by dissolution of the API in the dissolution medium, resulting in a faster drug release rate [1-2]. This mechanism was observed for all MET and PAR in BA prills, except for the 10% MET in BA prills as shown in Fig. 11b and 12b. Despite the lower drug load in the BA prills with 10% MET and consequently low potential to form a channel network in the matrix, 63% of the drug load was released in 1h compared to 37%, 32% and 49% release from BA prills containing 20%, 30% and 40% MET, respectively. This deviant dissolution profile was attributed to an inhomogeneous API distribution as demonstrated via X-ray tomography and Raman mapping. X-ray tomography showed that MET crystals (white regions in Fig. 13a) were preferentially located at the border of prills containing 10% MET, while at higher drug content the drug was homogeneously distributed throughout the prill. The inhomogeneous distribution of 10% MET in the BA matrix was confirmed by monitoring the intensity of a characteristic MET peak (737 cm^{-1}) relative to a characteristic BA peak (1,295 cm^{-1}) via Raman mapping (Fig. 14). A red colour corresponds to a high relative intensity, while a blue colour corresponds to a low relative intensity of MET demonstrating that the relative intensity of the typical MET peak decreased from the surface to the centre of a 10% MET in BA prill. These variations in relative intensity were not observed at higher drug loads as illustrated for a 30% MET in BA prill in Figure 14c. This inhomogeneous API distribution can be explained by the low viscosity of the 10% MET in BA molten mixture (Fig. 3) leading to higher mobility of MET particles after droplet formation and before solidification in comparison with higher MET drug load formulations and PAR formulations. It should also be noted that no complete drug release (maximum 94%) was obtained for 10% MET in BA prills as some MET crystals remained isolated in the BA matrix in comparison with the higher MET drug loaded prills.

Fig. 11a and 12a illustrate the influence of the FA chain length on drug release. The drug release rate increased when the FA chain length decreased as demonstrated by Vervaeck et al. [11], except for SA-based prills. The faster release from the SA matrix was linked to the higher porosity of this formulation as identified via X-ray tomography (Fig. 13b). Since the time needed to reach the FA crystallisation peak maximum during isothermal crystallisation 6°C below the melting temperature of the FA was comparable (10.1 ± 0.7 s) and fast for all 30% MET formulations (i.e. BA, SA, PA, MA), the origin of multiple pores in SA based formulations could not be explained by differences in crystallization rate and is therefore still under research.

As illustrated in Fig. 11, complete drug release of MET in demineralized water was obtained after 2.5 h up to 6 h depending on the drug load and FA chain length. On the other hand, 20% PAR prills (Fig. 12a) released 48% up to 95% within 24 h depending on the type of FA when demineralized water was used as dissolution medium. This slower and incomplete drug release was correlated with the more than 15 times lower water solubility of PAR in comparison with MET [2].

To evaluate the effect of pH and surfactants, the drug release profile was measured in phosphate buffer (pH 7.4), 0.1M HCl (pH 1) and 0.1% SLS solution. As seen in Fig. 12b, the addition of 0.1% SLS to the demineralized water medium or the use of a phosphate buffer increased

the drug release of a 20% PAR in BA prill from 48% to 71% and 75%, respectively. As demonstrated by Vervaeck et al., the effect of the phosphate buffer was the result of (partial) ionization of the carboxyl group of FA, which increased the matrix hydrophilicity [11]. Since this (partial) ionization was not achieved at pH 1 (0.1M HCl), the release profile was similar ($f_2 = 85\%$) with the profile obtained in demineralized water (pH 5.4). Although the SLS concentration was below the critical micellar concentration, the surfactant improved the wettability of the prills and as a result the release rate of PAR in the dissolution medium [1]. The combination of a phosphate buffer or 0.1% SLS solution as dissolution medium and a short chain FA, resulted in a complete drug release in less than 12 h and 16 h, respectively for 20% PAR in MA prills (Fig 12c). No significant effect of the dissolution medium on the release rate of MET formulations was observed, due to the high water solubility and fast channel network formation (data not shown).

No significant differences ($f_2 > 50$) in drug release profile were observed after storing MET and PAR prills during a 6 months period at low relative humidity (< 30%) at 25°C and 40°C. This is in accordance with the solid state analysis that did not reveal any transformations.

Although all prills had a similar size with a constant drug content per mass unit and the drug release profiles were reproducible, variations in the size of the cavity inside the prills could disturb volumetric capsule filling with a correct API dose. Therefore the variation in size of the cavity within each formulation was evaluated by calculation of the specific surface area of at least 10 prills based on X-ray tomography scanning images (Table 5). For all MET formulations, independent of drug load or FA chain length, the relative standard deviation was less than 10%. This method to relatively quantify the size of the cavity inside the prill was not applicable to PAR formulations. SEM images revealed that PAR prills have a rougher microscopic surface (Fig. 15) inducing a large variation in the calculated surface area. Despite the lack of a more suitable technique to quantify the cavity inside each individual prill, it was concluded that the presence of a cavity inside the prill is not problematic since the drug release profiles were reproducible and high speed camera images in combination with RHC measurements demonstrating the cavity arose due to shrinking during cooling without mass loss. Moreover, on an industrial scale droplets will be formed by the laminar jet break-up of a continuous flow by a vibrating nozzle system and subsequently being cooled during their falling motion in a cooling tower. Consequently, this will result in an even more homogeneous particle size distribution and droplet cooling [10, 36-37].

4. CONCLUSION

This study indicated that prilling of API/FA suspensions is a promising technique for the production of lipid based multi-particulate spherical dosage forms. In order to successfully prill API/FA suspensions, API powder needed to be sieved ($d_{90\ wet} \leq 60\mu m$) to prevent nozzle obstruction due to large or agglomerated API particles in the molten FA. Lab scale prilling equipment parts with a high probability of API sedimentation were modified to obtain prills with a relative drug content deviation ≤ 15% in function of processing time. The processability of API/FA suspensions was only limited by the viscosity of the molten mixture which was mainly affected by the size and shape of the API particles but was independent of the FA chain length. A lower API particle size and aspect ratio, resulted in a higher amount of particle-particle interactions and consequently a higher viscosity at equal drug load. Therefore MET and PAR formulations could be prilled up to a drug load of respectively, 40% and 20%. Although highly viscous formulations were no longer processable, a viscosity ≤ 0.01Pa.s resulted in an inhomogeneous API distribution in 10% MET in BA prills due to the high API mobility during droplet formation.

API/FA suspensions, always had a fast recrystallization of their FA fraction upon cooling, resulting in prills with an orifice at their surface which was connected to a cavity inside the prill dominated by the shrinking behavior of FA during solidification, without negatively influencing the reproducibility of the drug release. When enough MPT molecules were dissolved in the molten FA, the recrystallization of the FA was slowed down whereby the droplet solidification was no longer dominated by the shrinking behavior of FA resulting in completely solid and spherical prills despite an expulsion on their surface.

The collected API/FA suspension based prills were spherical (AR ≥ 0.895) with a smooth surface (sphericity ≥ 0.919) and a stable particle size of ± 2.3mm and 2.4mm for MET and PAR prills respectively, independent of the drug load and/or FA chain length. In vitro drug release evaluation revealed a faster drug release at higher drug load and shorter FA chain length. Due to the higher water solubility of MET, the *in vitro* drug release rate out of MET prills was higher and less susceptible to pH differences and/or surfactants present in the dissolution medium in comparison with PAR prills. Solid state characterization via XRD and Raman spectroscopy proved the preservation of API and FA crystallinity after thermal processing via prilling and during storage. Drug release of both MET and PAR prills was stable during 6m storage at 25°C and 40°C.

In future experiments upscaling of the prilling process will be studied on a system where droplets will be formed by the laminar jet break-up of a continuous flow by a vibrating nozzle system and subsequently being cooled during their falling motion in a cooling tower.

5. TABLES

Table 1. *Overview of API/FA suspensions used to evaluate the influence of drug load and type of FA on the processability.*

MET (x) and PAR (o) formulations					
FA	drug load (%)				processing temp (°C)
	10	20	30	40	$T_{melt\ FA}$ + 30°C
MA, C14		o	x		83
PA, C16		o	x		92
SA, C18		o	x		98
BA, C22	o x	o x	x	x	105

Table 2. *Particle size (d_{50}, d_{90} and span) and shape (aspect ratio) of both model APIs measured under dry and wet conditions, before and after sieving: MET – 50µm sieve, PAR – 150µm sieve*

API powder: size and shape									
measuring conditions		MET				PAR			
		d_{50} (µm)	d_{90} (µm)	span	AR	d_{50} (µm)	d_{90} (µm)	span	AR
dry	unsieved	110.6	277.3	2.26	0.731	25.3	505.0	20.69	0.714
	sieved	17.1	36.7	1.84	0.810	12.8	38.1	2.59	0.765
wet	unsieved	118.3	220.1	1.83	NA	42.2	75.6	1.41	NA
	sieved	33.4	60.4	1.76	NA	22.7	51.5	2.23	NA

Table 3. *Weighted average drug content of the two formulated batches and maximum relative drug content deviation of prills as a function of processing time at 6min intervals over a 1h period.*

drug content		
formulation	weighted average ± SD (%)	max relative deviation (%)
10% MET in BA	10.09 ± 0.18	3.60
20% MET in BA	19.09 ± 1.05	-12.91
30% MET in MA	29.78 ± 0.59	-4.81
30% MET in PA	30.14 ± 0.70	7.25
30% MET in SA	29.94 ± 0.58	4.21
30% MET in BA	29.28 ± 0.66	-9.02
40% MET in BA	40.36 ± 0.80	3.76
10% PAR in BA	10.60 ± 0.33	12.69
20% PAR in MA	20.29 ± 0.52	5.45
20% PAR in PA	20.81 ± 0.41	7.72
20% PAR in SA	21.31 ± 0.54	11.92
20% PAR in BA	21.26 ± 0.99	12.59

Table 4. *Overview of average particle size and shape of MET and PAR prills. No trends in function of drug load and/or FA chain length could be observed.*

MET prills				
	BA prills: influence of drug load			
	10	20	30	40
d_{50} ± SD (µm)	2.35 ± 0.02	2.31 ± 0.07	2.28 ± 0.05	2.21 ± 0.07
span	0.10	0.08	0.08	0.10
sphericity	0.93	0.93	0.94	0.94
aspect ratio	0.91	0.90	0.91	0.91
	30% MET prills: Influence of FA type			
	MA	PA	SA	BA
d_{50} ± SD (µm)	2.31 ± 0.02	2.32 ± 0.01	2.33 ± 0.04	2.28 ± 0.05
span	0.12	0.10	0.10	0.08
sphericity	0.94	0.94	0.94	0.94
aspect ratio	0.90	0.90	0.91	0.91

PAR prills				
	BA prills: influence of drug load			
	10*	20		
d_{50} ± SD (µm)	2.47	2.38 ± 0.06		
span	0.07	0.09		
sphericity	0.92	0.93		
aspect ratio	0.93	0.93		
	20% PAR prills: influence of FA type			
	MA	PA	SA	BA
d_{50} ± SD (µm)	2.44 ± 0.02	2.44 ± 0.02	2.40 ± 0.07	2.38 ± 0.06
span	0.09	0.09	0.09	0.09
sphericity	0.92	0.92	0.91	0.93
aspect ratio	0.91	0.91	0.91	0.93

* only 1 batch could be analyzed

Table 5. *Average specific surface area and relative standard deviation of at least 10 MET prills per formulation based on X-ray tomography image analysis.*

formulation	specific surfaca area (mm^{-1})	relative standard deviation (%)
10% MET in BA	3.30	8.85
20% MET in BA	3.25	4.25
30% MET in MA	3.40	2.72
30% MET in PA	3.27	4.53
30% MET in SA	3.89	3.54
30% MET in BA	3.06	3.60
40% MET in BA	3.94	6.13

6. FIGURES

Fig. 1. *Design of the modified Prilldrop device. a) melt reservoir b) reservoir heater and magnetic stirrer c) temperature sensor with feedback loop d) thermostated nozzle e) original nozzle heater f) extra nozzle heater g) valve h) needle (ID: 0.445 mm)*

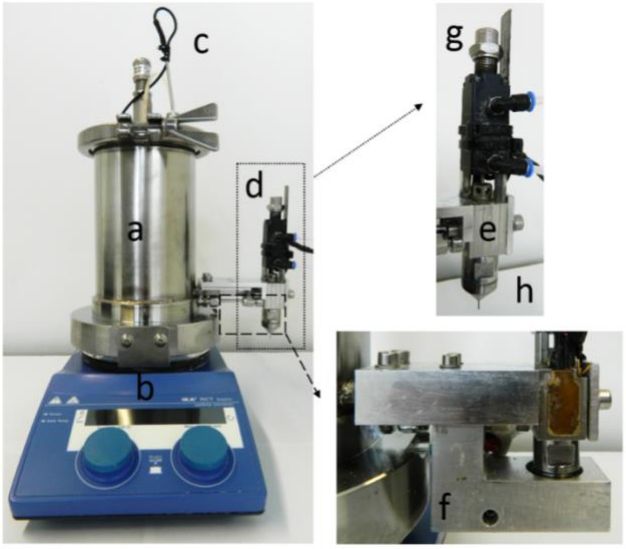

Fig 2. *Schematic overview of the final seamless nozzle*

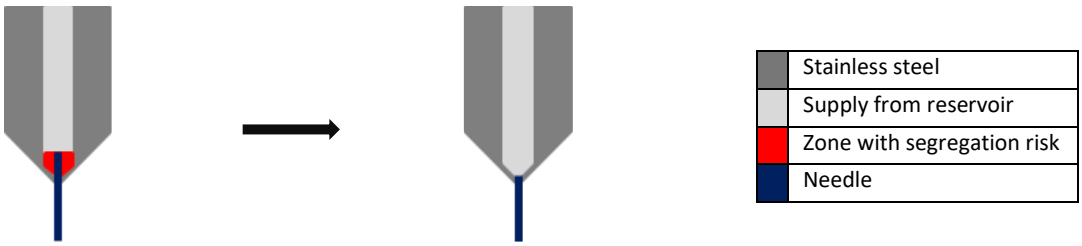

Fig 3. *Viscosity of API/BA suspensions and a 30% MPT in BA solution at processing temperature ($T_{melt\ FA}$ + 30°C) in function of shear rate*

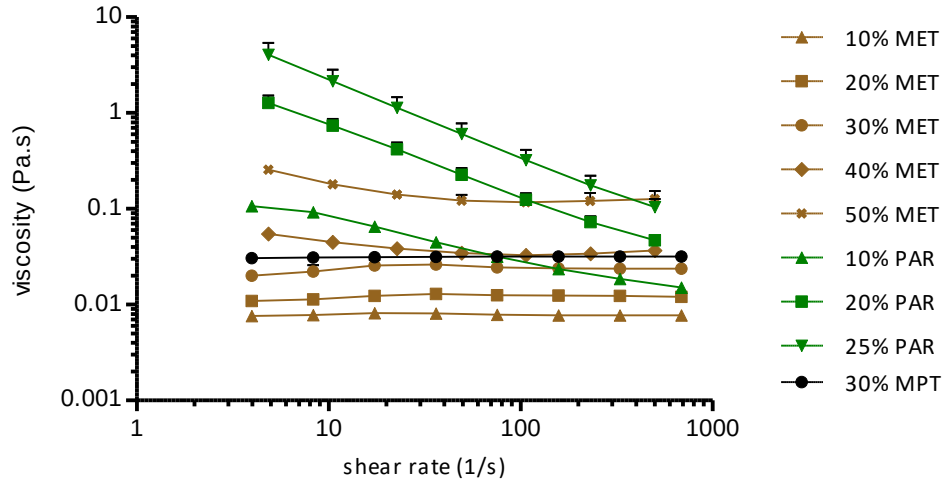

Optional figure: *viscosity of 30% MET in FA suspensions at processing temperature ($T_{melt\ FA}$ + 30°C) in function of shear rate (Ruwe ipv optimaal gladde platen)*

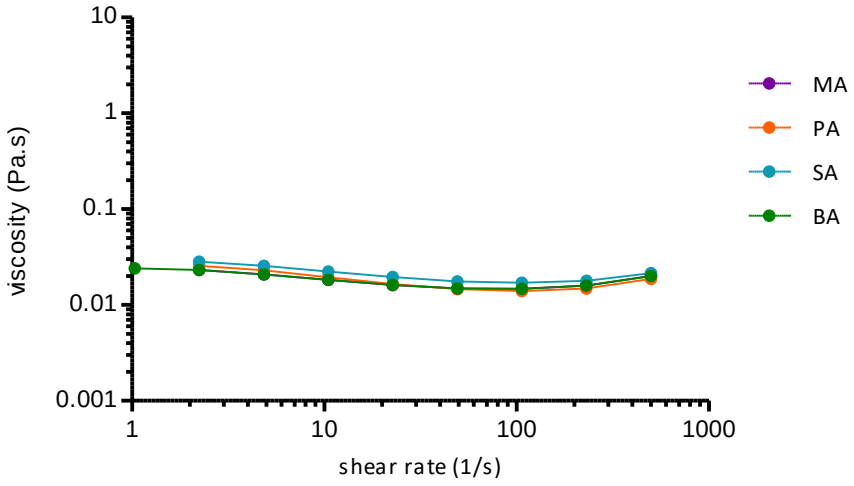

Fig 4. *SEM-images: sieved (left) MET (50µm) and (right) PAR (150µm) powder particles*

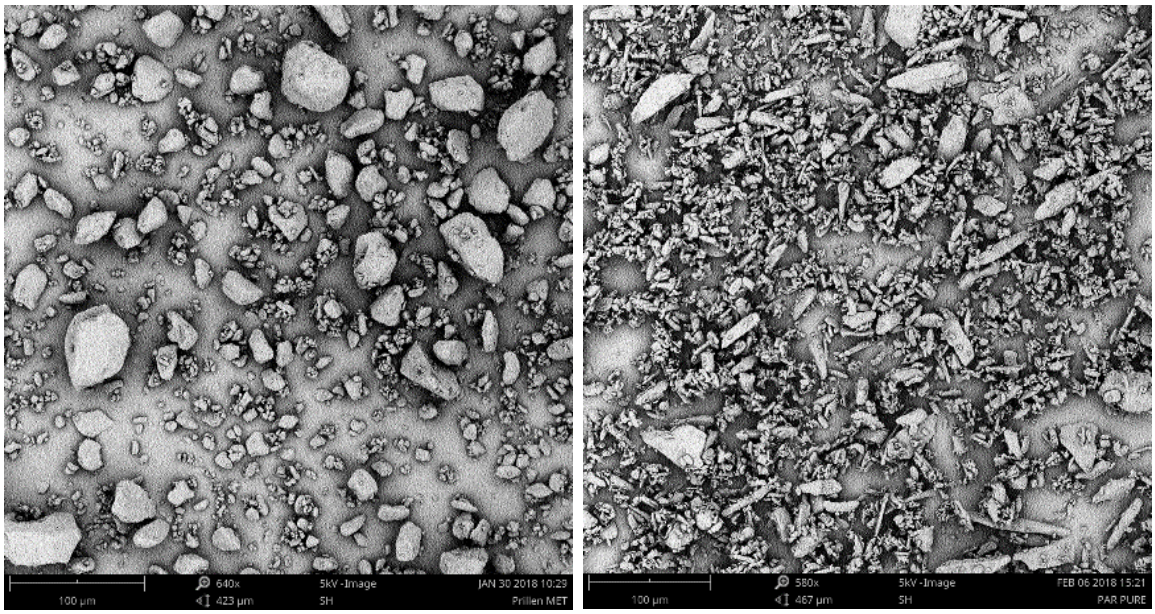

Fig. 5. *SEM-images: surface (a, c) and cross-section (b) of prills containing (a, b) 20% MET in BA and (c) 30% MPT in BA*

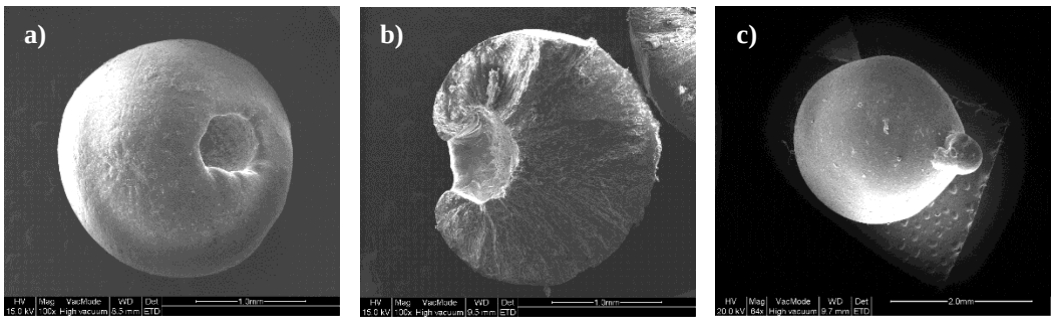

Fig. 6. Spherical droplet formation at the nozzle of a transparent 30% MPT in BA solution in function of time.

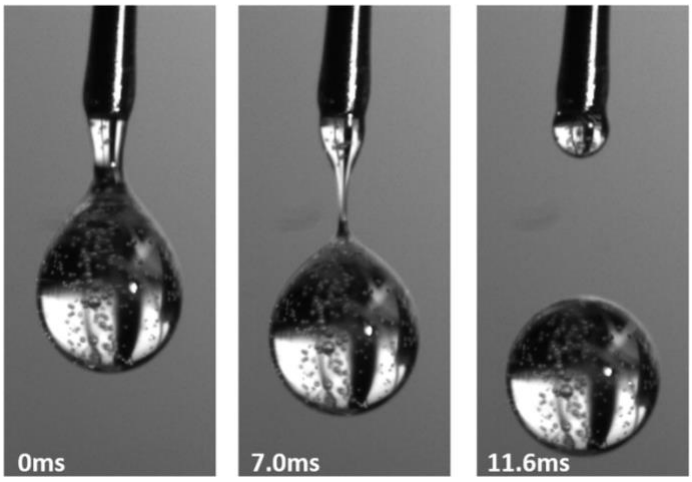

Fig. 7. Spherical droplet formation at the nozzle of an opaque 10% MET in BA suspension in function of time.

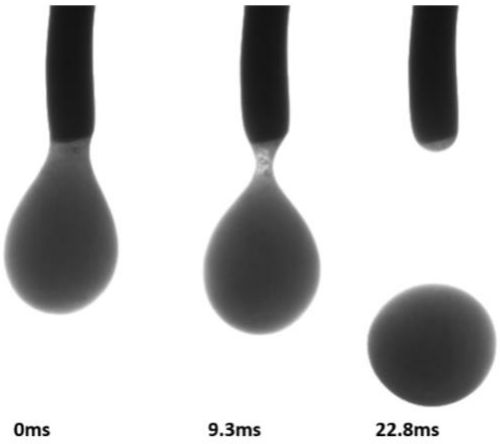

Fig. 8. *Solidification of a 30% MET in BA prill during fast solidification in liquid nitrogen.*

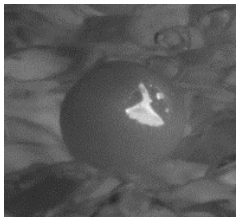

Fig. 9. *Formation of an expulsion at the surface of a 30% MPT in BA prill during fast solidification in liquid nitrogen.*

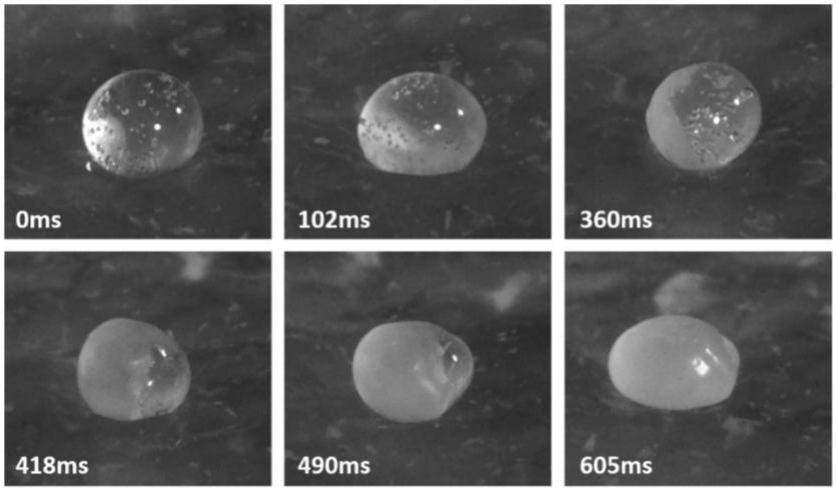

Fig. 10. Time needed to reach the BA crystallization peak maximum during isothermal crystallization as a measure for droplet solidification rate. Both API/BA suspensions and solutions with varying drug loads were analyzed at different crystallization temperatures.

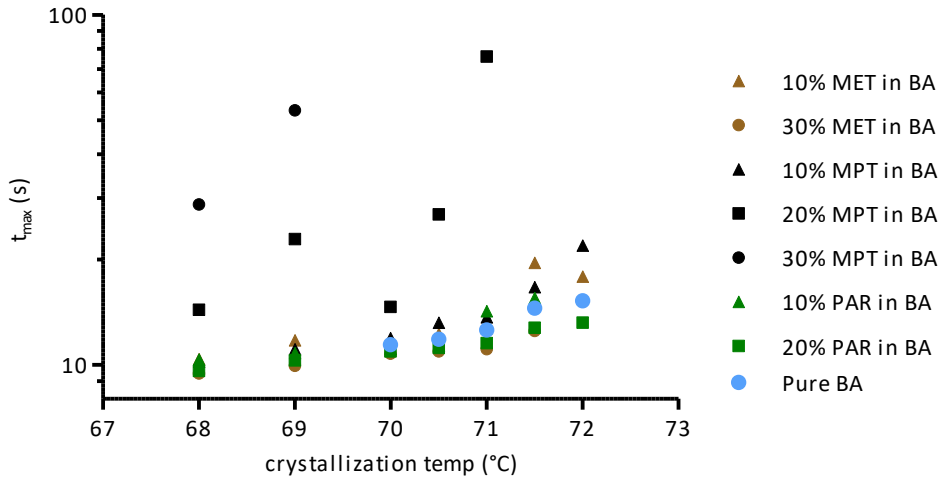

Fig. 11. *Mean dissolution profile (± SD) of MET prills in demineralized water in function of (a) FA chain length and (b) drug load.*

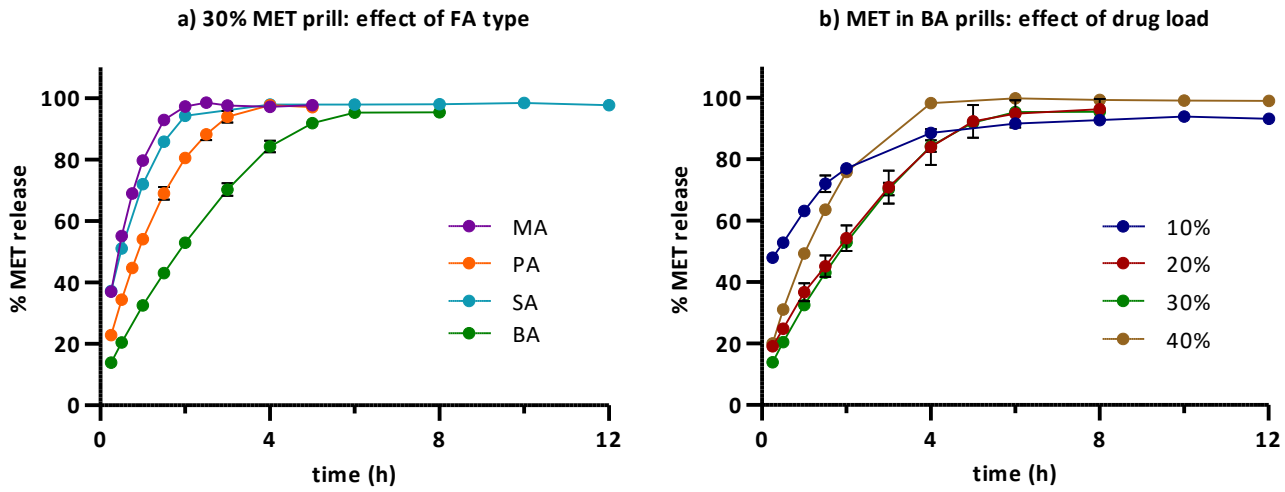

Fig. 12. *Mean dissolution profile (± SD) of PAR prills in function of (a) FA chain length in demineralized water, (b) drug load and (b,c) dissolution medium.*

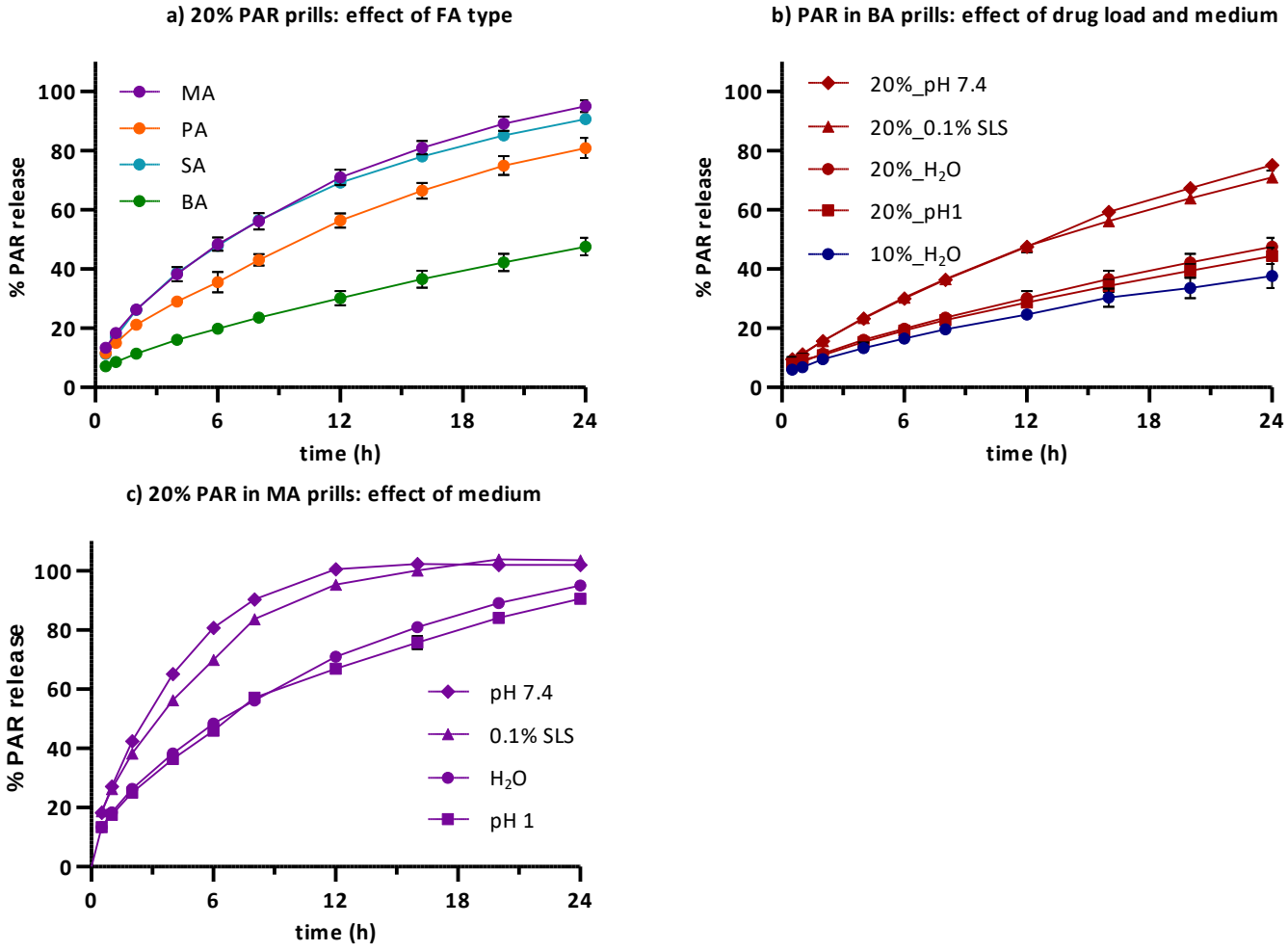

Fig. 13. *X-ray tomography cross section of a) 10% MET in BA prills with an inhomogeneous MET distribution b) 30% MET in SA prills with a high porosity*

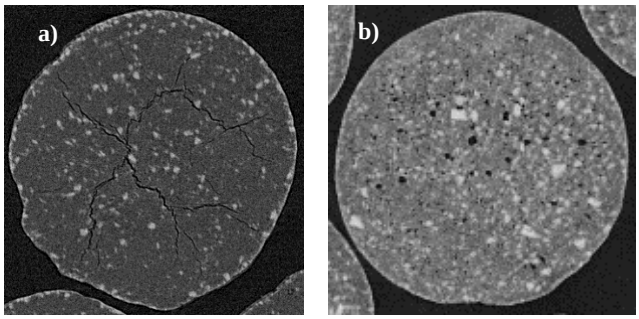

Fig. 14.

Visualization of MET distribution in 10% (a,b) and 30% (c) MET in BA prills via Raman mapping: going from the center to the border of a cross section from left to right with a 10x (a, c) or 50x (b) objective lens. A red colour corresponds to a high relative intensity (high MET content), while a blue colour corresponds to a low relative intensity (low MET content).

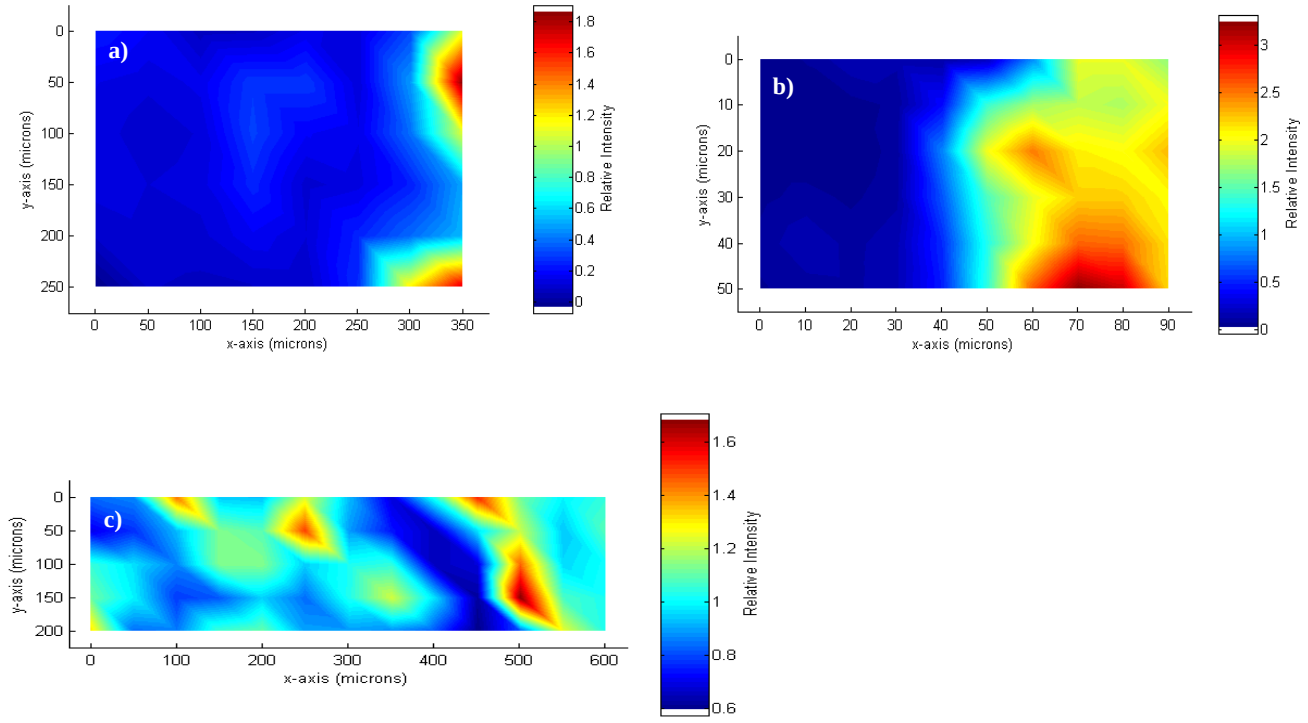

Fig. 15. *SEM images of a) smooth 30% MET in BA prill surface and b) rough 10% PAR in BA prill surface*

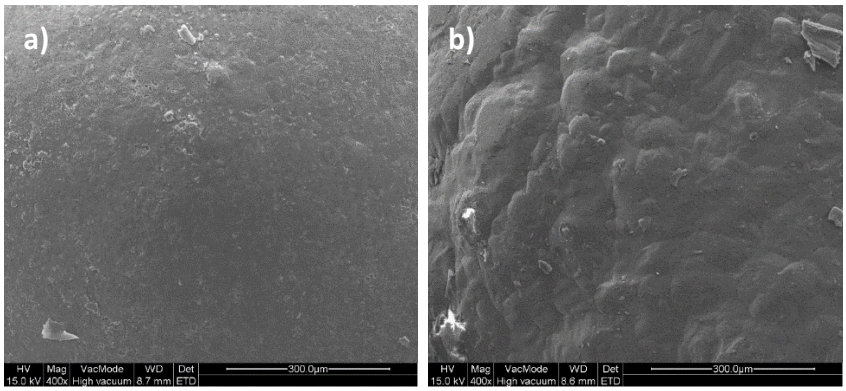

7. REFERENCES

1. Pivette P, Faivre V, Mancini L, Gueutin C, Daste G, Ollivon M, et al. Controlled release of a highly hydrophilic API from lipid microspheres obtained by prilling: analysis of drug and water diffusion processes with X-ray-based methods. J Control Release. 2012;158(3):393-402.
2. Rosiaux Y, Jannin V, Hughes S, Marchaud D. Solid lipid excipients - matrix agents for sustained drug delivery. J Control Release. 2014;188:18-30.
3. Jannin V, Musakhanian J, Marchaud D. Approaches for the development of solid and semi-solid lipid-based formulations. Adv Drug Deliv Rev. 2008;60(6):734-746.
4. Reitz C, Kleinebudde P. Solid lipid extrusion of sustained release dosage forms. Eur J Pharm Biopharm. 2007;67(2):440-448.
5. Becker K, Salar-Behzadi S, Zimmer A. Solvent-free melting techniques for the preparation of lipid-based solid oral formulations. Pharm Res. 2015;32(5):1519-1545.
6. Aleksovski A, Van Bockstal PJ, Roskar R, Sovany T, Regdon G, Jr., De Beer T, et al. Comparison of metoprolol tartrate multiple-unit lipid matrix systems produced by different technologies. Eur J Pharm Sci. 2016;88:233-245.
7. Vervaeck A, Monteyne T, Siepmann F, Boone MN, Van Hoorebeke L, De Beer T, et al. Fatty acids for controlled release applications: A comparison between prilling and solid lipid extrusion as manufacturing techniques. Eur J Pharm Biopharm. 2015;97(Pt A):173-184.
8. Passerini N, Qi S, Albertini B, Grassi M, Rodriguez L, Craig DQ. Solid lipid microparticles produced by spray congealing: influence of the atomizer on microparticle characteristics and mathematical modeling of the drug release. J Pharm Sci. 2010;99(2):916-931.
9. Martins RM, Siqueira S, Machado MO, Freitas LA. The effect of homogenization method on the properties of carbamazepine microparticles prepared by spray congealing. J Microencapsul. 2013;30(7):692-700.
10. Sequier F, Faivre V, Daste G, Renouard M, Lesieur S. Critical parameters involved in producing microspheres by prilling of molten lipids: from theoretical prediction of particle size to practice. Eur J Pharm Biopharm. 2014;87(3):530-540.
11. Vervaeck A, Saerens L, De Geest BG, De Beer T, Carleer R, Adriaensens P, et al. Prilling of fatty acids as a continuous process for the development of controlled release multiparticulate dosage forms. Eur J Pharm Biopharm. 2013;85(3 Pt A):587-596.
12. Rahmanian N, Naderi S, Supuk E, Abbas R, Hassanpour A. Urea Finishing Process: Prilling Versus Granulation. Procedia Engineering. 2015;102(Supplement C):174-181.
13. Rahmanian N, Homayoonfard M, Alamdari A. Simulation of urea prilling process: an industrial case study. Chemical Engineering Communications. 2013;200(6):764-782.
14. Rahamnian N, Homayoonfard M. A comparison of co-current and counter-current modes of operation in urea prilling tower. In: Ismail L, Azizli KA, Murugesan T, Ganguly S, Uemura Y, editors. Proceedings of the International Conference on Process Engineering and Advanced Materials 2012-Icpeam 2012. Advanced Materials Research. 917. Stafa-Zurich: Trans Tech Publications Ltd; 2014. p. 199-208.
15. Mehrez A, Ookawara S, Ali AHH, Suzuki M. A numerical study on cooling-solidification process of urea particles in prilling tower. Journal of Chemical Engineering of Japan. 2014;47(8):628-634.
16. Desai D, Wong B, Huang Y, Ye Q, Tang D, Guo H, et al. Surfactant-mediated dissolution of metformin hydrochloride tablets: wetting effects versus ion pairs diffusivity. J Pharm Sci. 2014;103(3):920-926.
17. A. Granberg R, Rasmuson Å. Solubility of Paracetamol in Pure Solvents. J Chem Eng Data. 1999;44(6):1391-1395.
18. Barnes HA. A review of the slip (wall depletion) of polymer solutions, emulsions and particle suspensions in viscometers: its cause, character, and cure. Journal of Non-Newtonian Fluid Mechanics. 1995;56(3):221-251.
19. Marchesini F, Naccache M, Abdu A, Alicke A, De Souza Mendes P. Rheological characterization of yield-stress materials: Flow pattern and apparent wall slip2015. 53883 p.
20. De Souza Mendes P, Alicke A, Thompson R. Parallel-plate geometry correction for transient rheometric experiments2014. 52721 p.
21. Mueller S, Llewellin EW, Mader HM. The rheology of suspensions of solid particles. Proceedings of the Royal Society A: Mathematical, Physical and Engineering Sciences. 2010;466(2116):1201-1228.
22. Shah VP, Tsong Y, Sathe P, Liu JP. In vitro dissolution profile comparison--statistics and analysis of the similarity factor, f2. Pharm Res. 1998;15(6):889-896.
23. Vervaeck A, Monteyne T, Saerens L, De Beer T, Remon JP, Vervaet C. Prilling as manufacturing technique for multiparticulate lipid/PEG fixed-dose combinations. Eur J Pharm Biopharm. 2014;88(2):472-482.
24. Del Gaudio P, Russo P, Rosaria Lauro M, Colombo P, Aquino RP. Encapsulation of ketoprofen and ketoprofen lysinate by prilling for controlled drug release. AAPS PharmSciTech. 2009;10(4):1178-1185.
25. Garti N, Sato K. Crystallization and polymorphism of fats and fatty acids. New York: Marcel Dekker, Inc.; 1988.

26. Masschaele B, Dierick M, Denis V, Boone M, Brabant L, Pauwels E, et al. HECTOR: a 240kV micro-CT setup optimized for research. Journal of Physics Conference Series. 2013;463.
27. Nutan MTH, Reddy IK. General Principles of Suspensions. In: Kulshreshtha AK, Singh ON, Wall GM, editors. Pharmaceutical Suspensions: Springer; 2010. p. 39-65.
28. 2.9.40. Uniformity of dosage units. In: Europe Co, editor. European Pharmacopoeia 902016. p. 372-375.
29. paper Xw. 10 Ways to...Control Rheology by Changing Particle Properties (Size, Zeta Potential and Shape).
30. Genovese DB. Shear rheology of hard-sphere, dispersed, and aggregated suspensions, and filler-matrix composites. Adv Colloid Interface Sci. 2012;171:1-16.
31. Vervaeck A. Prilling of fatty acids as innovative technology for oral controlled release multiple-unit systems. 2015.
32. Wu Y, Bao C, Zhou Y. An Innovated Tower-fluidized Bed Prilling Process. Chin J Chem Eng. 2007;15(3):424-428.
33. Brockmann R, Demmering G, Kreutzer U, Lindemann M, Plachenka J, Steinberner U. Fatty Acids. Ullmann's Encyclopedia of Industrial Chemistry. 40. 6th ed. Weinheim2000.
34. Vibrational spectroscopic aspects of polymorphism and phase transition of fats and fatty acids. In: Kobayashi M, editor. Crystallization and Polymorphism of Fats and Fatty Acids. 31. New York: Marcel Dekker, Inc.; 1988. p. 139-187.
35. Singleton WS, Ward TL, Dollear FG. Physical properties of fatty acids. I. Some dilatometric and thermal properties of stearic acid in two polymorphic forms. J Am Oil Chem Soc. 1950;27(4):143-146.
36. Haas PA. Formation of uniform liquid drops by application of vibration to laminar jets. Ind Eng Chem Res. 1992;31(3):959-967.
37. Pivette P, Faivre V, Daste G, Ollivon M, Lesieur S. Rapid cooling of lipid in a prilling tower. Journal of Thermal Analysis and Calorimetry. 2009;98(1):47.